Generalized periodic surface model and its application in designing fibrous porous media

Wei Huang, Sima Didari, Yan Wang and Tequila A.L. Harris
Woodruff School of Mechanical Engineering, Georgia Institute of Technology, Atlanta, Georgia, USA

Received 12 March 2013
Revised 31 October 2013
Accepted 15 February 2014

Abstract

Purpose – Fibrous porous media have a wide variety of applications in insulation, filtration, acoustics, sensing, and actuation. To design such materials, computational modeling methods are needed to engineer the properties systematically. There is a lack of efficient approaches to build and modify those complex structures in computers. The paper aims to discuss these issues.

Design/methodology/approach – In this paper, the authors generalize a previously developed periodic surface (PS) model so that the detailed shapes of fibers in porous media can be modeled. Because of its periodic and implicit nature, the generalized PS model is able to efficiently construct the three-dimensional representative volume element (RVE) of randomly distributed fibers. A physics-based empirical force field method is also developed to model the fiber bending and deformation.

Findings – Integrated with computational fluid dynamics (CFD) analysis tools, the proposed approach enables simulation-based design of fibrous porous media.

Research limitations/implications – In the future, the authors will investigate robust approaches to export meshes of PS models directly to CFD simulation tools and develop geometric modeling methods for composite materials that include both fibers and resin.

Originality/value – The proposed geometric modeling method with implicit surfaces to represent fibers is unique in its capability of modeling bent and deformed fibers in a RVE and supporting design parameter-based modification for global configuration change for the purpose of macroscopic transport property analysis.

Keywords Computer-aided design, Fibrous porous media, Geometric modelling, Implicit surface, Periodic surface model

Paper type Research paper

Nomenclature

$a =$	the x-coordinate of a basis vector	$\mathbf{G} =$	a basis vector of the variable phase without homogeneous coordinate
$b =$	the y-coordinate of a basis vector	$\mathbf{G}^* =$	a basis vector of the variable phase with zero homogeneous coordinate
$c =$	the z-coordinate of a basis vector	$\mathbf{H} =$	a basis vector of the fundamental or generalized PS model without homogeneous coordinate
$D =$	the diameter of the rod surface		
$diff =$	difference		
diff–max =	the maximum difference		
$f =$	the scale parameter of the variable phase	$\mathbf{H}^* =$	a basis vector of the fundamental or generalized PS model with zero homogeneous coordinate

This work is supported in part by the National Science Foundation under the grant numbers CMMI-1001040 and CMMI-0928093.

Engineering Computations: International Journal for Computer-Aided Engineering and Software
Vol. 32 No. 1, 2015
pp. 7-36

0264-4401
DOI 10.1108/EC-03-2013-0085

$\mathbf{I}=$	identity matrix	$U=$	the total potential energy
$i=$	the ith fiber	$u=$	the periodic moment of a variable phase
$j=$	the jth fiber		
$L=$	the scale of the fundamental or generalized periodic surface model	$V=$	the superficial velocity
		$v=$	the shift distance between two cross sections
$M=$	the degree of a periodic surface model under a scale parameter	$w=$	the homogeneous coordinate of the location vector
$l=$	the lth scale parameter of the fundamental or generalized periodic surface model	$x=$	the x-coordinate of the location vector
		$y=$	the y-coordinate of the location vector
$m=$	the mth basis vector under a scale parameter	$z=$	the z-coordinate of the location vector
$\max=$	the maximum value		
$\min=$	the minimum value	$\alpha=$	the phase of a basis plane
$n=$	the number of fibers	$\beta=$	the phase of a variable phase of the generalized PS model
$\mathbf{p}=$	a basis vector of the fundamental or generalized PS model	$\boldsymbol{\alpha}^*=$	the phase vector of a basis plane
$\nabla P=$	the pressure drop per unit length through the porous material	$\boldsymbol{\beta}^*=$	the phase vector of a variable phase of the generalized PS model
$\mathbf{q}=$	a basis vector of the variable phase		
$\mathbf{R}=$	the rotation matrix for the generalized PS model	$\eta=$	fluid viscosity
		$\theta=$	rotation about the y-axis
$\mathbf{r}=$	location vector with homogeneous coordinate	$K=$	permeability
		$\kappa=$	the scale parameter
$S=$	the scale of the phase of the generalized periodic surface model	$\mu=$	the periodic moment of the fundamental or generalized periodic surface model
$s=$	the sth scale parameter of the phase of the generalized periodic surface	$\xi=$	the components of the rotation matrix for the generalized PS model
$\mathbf{T}=$	translation matrix for the generalized PS model	$\psi=$	the function of the fundamental or generalized periodic surface model
$T=$	the degree of the phase of the generalized periodic surface model under a scale parameter	$\Omega=$	the volume of intersection portion among fibers
$\mathbf{t}=$	translation vector	$\omega=$	rotation about the z-axis
$t=$	the tth basis vector of the phase under a scale parameter		

1. Introduction

Porous media have recently received much attention in industry, such as in power generation, biomedical engineering, apparel fabrication, and automotive and aerospace manufacturing. This popularity is largely because of its superior properties compared to solid counterparts including higher strength-to-weight ratio and porosity (i.e. surface-area-to-volume ratio). A porous medium is typically made of stationary solid in the form of a matrix of interconnected pores. When the solid component is

formed by an assembly of fibers as webs and sheets, the medium is called fibrous porous. Fibrous porous media can be in either woven or non-woven form. For woven fibrous structures, curved fibers are knitted in regular patterns so that they are mechanically combined and fixed by friction at the locations where they contact, as shown in Figure 1. For non-woven fibrous structures, fibers are naturally packed and mechanically, thermally or chemically bonded. One example is shown in Figure 2. Because of their ease of fabrication, fibrous porous media have become very important materials in industry. Particularly, thanks to their good structural stability as well as unique thermal and electrical properties of certain fibers, non-woven fibrous porous media have become a preferred choice of materials in many applications including insulation, filtration, acoustics, sensing, and actuation.

Fibrous porous media can be composite materials that have complex structures. The gas diffusion layer (GDL) in Figure 2 from our experimental work is used in the polymer electrolyte membrane fuel cells (PEMFCs). The GDL consists of packed cylindrical carbon fibers with a polymer binder added, resulting in a structure that allows for the permeation of gases. GDLs are thin sheets of carbon papers consisting of randomly distributed fibers. The fibers have a diameter of 6-10 μm and a length of 10-20 mm. Other non-woven fibrous porous media have similar structures .

To obtain higher power densities in PEMFC, we need to increase the mass transfer rate and the concentration of reactants which are linked to the GDL transport properties. Computational fluid dynamics (CFD) tools are usually used to optimize the PEMFC's performance based on the GDL transport characteristics such as permeability and tortuosity. In such analyses, only a small portion of the physical domain, called representative volume element (RVE), is modeled. A RVE can be as small as the one in which simulation result is representative and can be generalized to the entire domain.

Because of the high degree of irregularity and complexity in the porous geometry, modeling porous media is a challenging task. The commonly used parametric surface modeling methods with local shape control are inefficient because a large number of control points are required to capture the complex topology. Although most of these methods are able to efficiently build individual fibers or particles with simple shapes

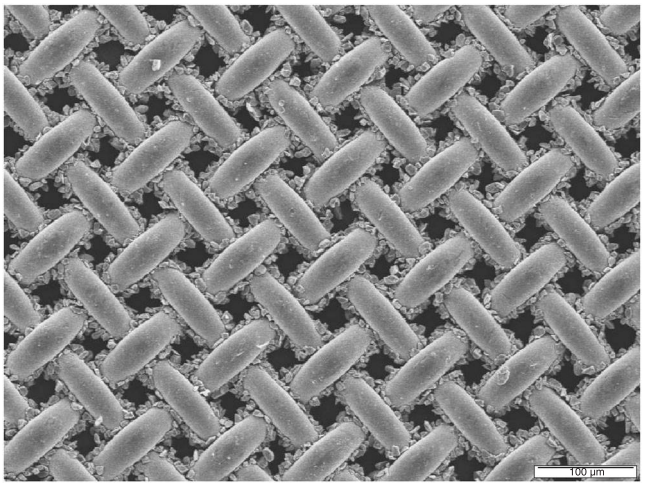

Figure 1.
An example of woven fibrous media (courtesy of AirScape Inc.)

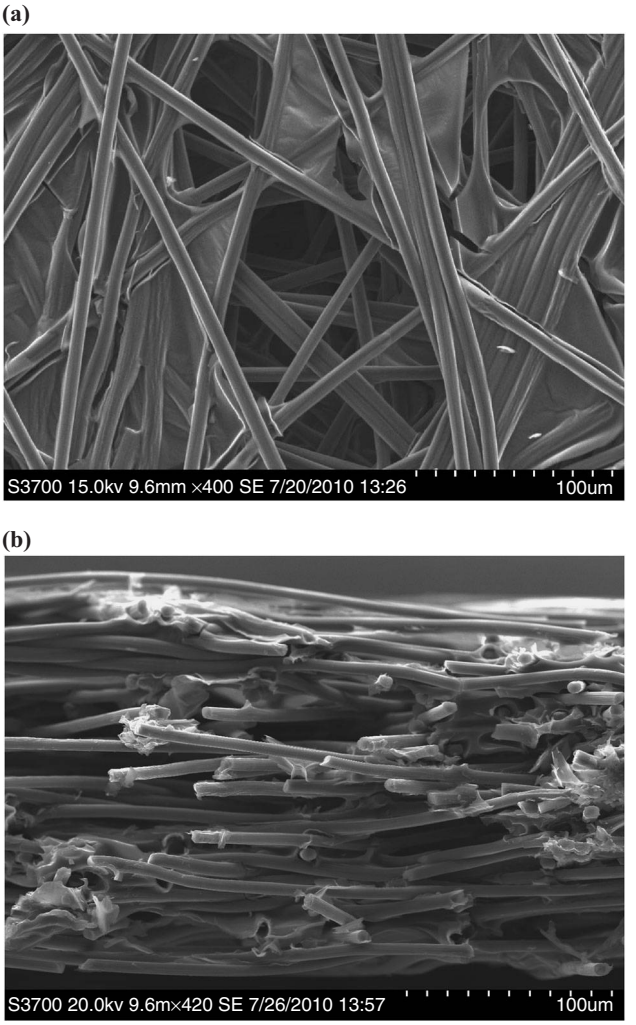

Figure 2.
Scanning electron microscope images of Toray 90 GDL

Notes: (a) Top view; (b) side view (cross-sectional view)

such as cylinders and spheres, it is difficult for them to build more complex and irregular shapes and at the same time control the overall porosity of the RVE with dozens or even hundreds of fibers or particles. In addition, RVEs typically require flexible domain sizes so that geometries can be modified based on simulation needs. An effective approach to build geometries that automatically satisfy the periodic boundary condition is desirable for the ease of modifying the size of RVEs.

In this paper, we propose a modeling approach to represent both woven and non-woven fibrous porous media based on the extension of a previously developed periodic surface (PS) model (Wang, 2007a, b, 2009; Qi and Wang, 2009). This new surface model allows us to efficiently build randomly distributed or patterned fibers, both straight and bent, in a RVE. The original PS model is generalized to provide more degrees of

freedom to control the complexity of shapes. From the implicit surface of generalized PS model, a mesh representation of fibers in a RVE can be generated and imported into CFD tools for analysis. Alternatively, geometric information such as medial axes, radius, and curvature of fibers can be imported into mesh generation tools to create mesh models.

In the remainder of the paper, we give a brief overview of geometric modeling of porous media in Section 2, where the original PS model is also introduced. In Section 3, the PS model is used to model straight fibers. In Section 4, the PS model is generalized and its corresponding transformation operations are introduced. In Section 5, we describe the method of modeling bent fibers based on the generalized PS model. In Section 6, a physics-based empirical force field method to model deformation of fibers is introduced. In Section 7, the detailed implementation process of the proposed method is described and demonstrated.

2. Literature review

Geometric modeling methods for porous media can be categorized into image-based and geometry-based approaches. In this section, a detailed overview of existing literature is provided. The organization of the review is shown in Figure 3.

2.1 Image-based approaches

For the image-based approaches, three-dimensional (3D) images, as the implicit representation of geometries, are directly obtained by scanning structures in a non-destructive way. Some existing scanning methods include transmission microscopy (Flegler, 1993), scanning tunneling electron microscopy (Stroscio and Kaiser, 1992), synchrotron-based tomography (Kinney and Nichols, 1992), confocal microscopy (Fredrich *et al.*, 1995), and computed microtomography (μCT) (Dabbs and Aksay, 1996; Bentz *et al.*, 2000). The discrete voxels in the images can be used directly for analysis and rapid prototyping (Strozzi *et al.*, 2009).

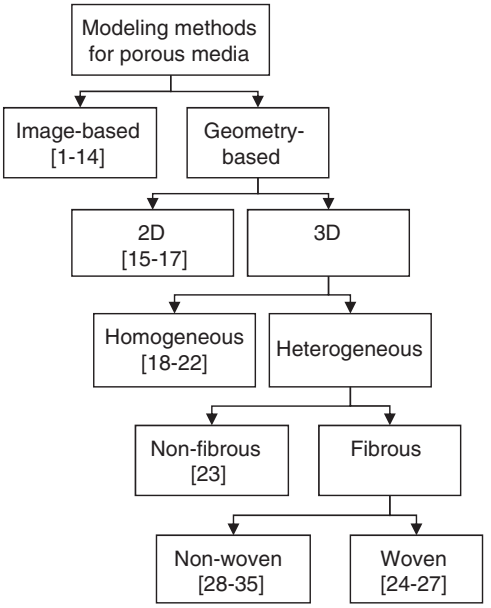

Figure 3.
The organization of literature review

For tissue engineering, Sun *et al.* (2005) generated the boundary representation (B-Rep) of porous systems from voxels. Zeng *et al.* (2000) modeled porous structures with predominant axis, such as yarns, by acquiring the successive cross-section images along the axis and then tracking geometric features of interstices (the void space). Some research efforts were only focused on fibrous porous media, where 3D models were reconstructed based on 2D imaging of actual fibers in either the woven or non-woven form. In the automated serial sectioning technique (Jaganathan *et al.*, 2008; Vaughan and Brown, 1996; Desplentere *et al.*, 2005), 2D images were taken at different sections of fibrous materials and the 3D geometry was reconstructed from these 2D images.

The image-based methods require advanced equipment and lengthy time to reconstruct the 3D micro-structure based on the taken images. Although imaging techniques accurately capture the geometry of actual structures, the models are hardly modifiable, which provides little value for the purpose of design. Moreover, the conversion from imaging data to B-Rep functions is a challenging task.

2.2 Geometry-based approaches

Geometry-based approaches, on the contrary, construct models based on closed-form mathematical functions. Since the functions are much easier to control than discrete voxels, these methods apparently provide more flexibility in the sense of design. Early research efforts simplified the 3D geometric modeling problem to a 2D one with the assumption of parallel fiber orientation so that only a 2D cross-section profile is modeled (Brown, 1984, 1993; Herman *et al.*, 2006). This simplification is proved effective in accelerating the simulation of fluid flow in 2D. However, to obtain more accurate simulation results, modeling 3D porous structure is apparently essential.

In porous media, the structures are called spatially homogeneous if the pores have the same size and shape; otherwise, they are called spatially heterogeneous. For spatially homogeneous porous media, the structures can be controlled globally since the pores have the same size and shape and therefore are periodic. Cheah *et al.* (2003a, b) used polyhedral shapes in modeling biological tissues. Chow *et al.* (2007) proposed a layer-based approach with 2D Voronoi tessellation to degrade the 3D problem to a 2D one. Kou and Tan (2010a, b) presented a modeling method for porous structures with graded porosities and pore distributions based on stochastic Voronoi diagram and B-Spline representation. Schroeder *et al.* (2003) proposed a representation method to effectively unify model density and porosity using stochastic geometry.

For spatially heterogeneous porous media, because of the variety of the sizes and shapes of the pores, local control of the pores is needed. Few geometry-based methods were established for spatially heterogeneous non-fibrous porous structures. Kou and Tan (2010a, b) used Voronoi tessellation to partition the space into a collection of compartments. Randomly selected compartments are merged together to obtain boundary polygons, the vertices of which are then used as control points of closed B-Spline curves. These B-Spline curves therefore represent the boundaries of the irregular-shaped pores in 2D.

Particularly for spatially heterogeneous fibrous porous media, several geometry-based modeling methods have been developed. For woven fibrous structures, curved fibers subject to interacting forces need to be modeled. (Peirce, 1937) modeled woven fibers with circular arcs connected by straight line segments. Hewitt *et al.* (1995) approximated fibers in woven composite materials by discrete but connected rectangular blocks. Turana and Baser (2010) used B-Spline to represent the central

curves of the woven fibers. Smith and Chen (2008) used differential equations to construct woven compressible structures without intersection among fibers.

Non-woven spatially heterogeneous fibrous structures are either non-layered such as yarn tows in textile, or layered such as GDLs. Non-layered fibrous structures were constructed by simply combining B-Rep models of individual fibers. Lin and Newton (1999) used cubic B-spline curves to represent the central curves of the fibers in 3D and generated the surface or solid model using sweep operations. Sreprateep and Bohez (2006) used non-uniform rational B-Spline to generate the central curves of the fibers in yarns and similarly built the solid model of fibers with sweep operations. Sun *et al.* (2001) used the commercial CAD software Pro/Engineer to build solid model of woven composite materials for stress and deformation analysis.

To model layered fibrous structures, fibers are usually inserted into the model one by one following certain levels of statistical distributions, either as aligned, layered, or random structures. For the aligned structure (Brown, 1984, 1993; Herman *et al.*, 2006; Chen and Papathanasiou, 2005), fibers are only distributed in parallel or perpendicular patterns with respect to one direction. For the layered structure (Hamilton, 2005; Wang *et al.*, 2006; Van Doormaal and Pharoah, 2009), fibers are built in a layer-by-layer pattern and randomly oriented within each layer so that no intersection exists among the fibers. In the random structure (Schulz *et al.*, 2007), the fibers are oriented randomly in all three spatial directions. These methods can only construct straight fibers with the simple cylindrical shape without intersections, which affects the accuracy of simulation.

In summary, existing geometric modeling methods for fibrous porous media are not efficient in constructing and modifying complex structures for the purpose of design of material properties in RVEs. Although B-Rep based parametric surface models are straight-forward, the disadvantage is that a large number of control points are involved and therefore it is hard to globally control the shapes of fibers. In design of material properties, local shape control of fibers is not important. Rather, modifying the overall structure with easily controllable parameters in a RVE and relating the values of parameters to the physical properties enable design engineers to establish structure-property relationships easily.

2.3 PS model

In this paper, we propose an implicit surface approach to model woven and non-woven fibrous porous structures. This is based on a generalized PS model as an extension of the original PS model (Wang, 2007a, b, 2009). Because of its periodic and implicit nature, the PS model can be used to represent porous structures at micro- and bulk scales. The implicit surface allows us to build 3D porous models more efficiently than explicit methods. Its periodic nature makes it more convenient in modeling self-repeating geometry. By simply increasing or decreasing the number of periods for the RVE, the size of the model will be enlarged or shrunk with more or less fibers included, which is important in modeling RVEs.

The PS model has the implicit form and is defined as:

$$\psi(\mathbf{r}) = \sum_{l=1}^{L} \sum_{m=1}^{M} \mu_{lm} \cos\left(2\pi\kappa_l\left(\mathbf{p}_m^T \cdot \mathbf{r}\right)\right) = 0 \tag{1}$$

where κ_l is the scale parameter:

$$\mathbf{p}_m = [a_m, b_m, c_m, \alpha_m]^T \tag{2}$$

is a basis vector, such as one of:

$$\{\mathbf{p}_m\} = \left\{ \begin{bmatrix}0\\0\\0\\1\end{bmatrix} \begin{bmatrix}1\\0\\0\\1\end{bmatrix} \begin{bmatrix}0\\1\\0\\1\end{bmatrix} \begin{bmatrix}0\\0\\1\\1\end{bmatrix} \begin{bmatrix}1\\1\\0\\1\end{bmatrix} \begin{bmatrix}1\\0\\1\\1\end{bmatrix} \begin{bmatrix}0\\1\\1\\1\end{bmatrix} \begin{bmatrix}1\\-1\\0\\1\end{bmatrix} \begin{bmatrix}-1\\0\\1\\1\end{bmatrix} \cdots \right\} \tag{3}$$

which represents a basis plane in the Euclidean space, and α_m corresponds to the phase of the basis plane defined in $\mathbf{p}_m$. In addition, $\mathbf{r} = [x, y, z, w]^T$ is the location vector with homogeneous coordinates, and μ_{lm} is the periodic moment. We assume $w = 1$ if not explicitly specified. The degree, M, of $\psi(\mathbf{r})$ in Equation (1) is defined as the number of unique vectors in the basis vector set $\{\mathbf{p}_m\}$. The scale, L, of $\psi(\mathbf{r})$ is defined as the number of unique scale parameters in $\{\kappa_l\}$. We can assume scale parameters as natural numbers ($\kappa \in \mathbb{N}$).

Figure 4 lists some examples of PS models. Triply periodic minimal surfaces, such as P-, D-, G-, and I-WP cubic morphologies that are frequently referred to in chemistry and polymer literature, can be adequately approximated. Besides the cubic phase, other mesophase structures such as spherical micelles, lamellar, rod-like hexagonal phases can also be modeled.

3. Modeling straight fibers using PS model

In non-woven fibrous porous structures, the fibers typically have circular cross-sections and much less bent than the ones in woven fibrous porous structures. Thus, their geometries can be approximately regarded as cylindrical shapes. The rod surface model as shown in Figure 4 is a good approximation of cylinders. Therefore it can be

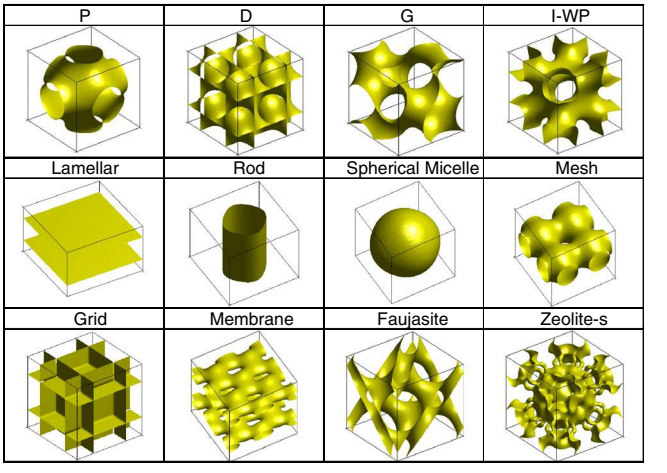

Figure 4.
Periodic surface models of cubic phase and mesophase structures

Source: Wang (2009)

used to model the fiber geometry. How to build the rod surface by the PS model is explained as follows.

The PS model:

$$\psi(x,y,z) = 4\cos(2\pi x) + 4\cos(2\pi y) + 3 = \psi_0 \tag{4}$$

represents a rod surface with the central axis along the z-axis direction, which is periodic in both x- and y-axis directions with the periodicity of 1. The corresponding parameters are $L=1$, $M=3$, $\mu_{11}=4$, $\mu_{12}=4$, $\mu_{13}=3$, $\kappa_1=\kappa_2=\kappa_3=1$, $\mathbf{p}_1=[1\ 0\ 0\ 0]^T$, $\mathbf{p}_2=[0\ 1\ 0\ 0]^T$, $\mathbf{p}_3=[0\ 0\ 0\ 0]^T$. For rod surfaces oriented along the x- and y-axes, the respective basis vectors are $\mathbf{p}_1=[0\,1\,0\,0]^T$, $\mathbf{p}_2=[0\,0\,1\,0]^T$, $\mathbf{p}_3=[0\,0\,0\,0]^T$ and $\mathbf{p}_1=[1\,0\,0\,0]^T$, $\mathbf{p}_2=[0\,0\,1\,0]^T$, $\mathbf{p}_3=[0\,0\,0\,0]^T$. With these parameters, the rod surfaces can approximate the geometry of cylinders well and can therefore be utilized to model straight fibers. The fibers are modeled in a RVE or a cube that is large enough to represent the properties of fibrous porous media. In this paper, the normalized size of the cube for the rod surface model is $x \in [0, 1]$, $y \in [0, 1]$, and $z \in [0, 1]$. There is only one rod surface defined by Equation (4) in the cube. Later in this section, we will show how to add more rod surfaces in the RVE. Notice that to better represent cylindrical shapes with higher accuracy, more terms can be introduced into Equation (4) at the cost of computation. Figure 5 illustrates the PS model of a rod surface in the RVE and the difference between the cross section of the rod surface and a circle. As the isovalue ψ_0 in Equation (4) changes, the diameter of the rod surface changes correspondingly.

As shown in Figure 5, the diameter of the fiber can be approximated by the distance between the positions with the maximum and minimum y-coordinate values in the cross section of the rod. That is, $D = Y_{\max} - Y_{\min}$. If we set $\psi(x,y,z) = \psi_0$ with a constant isovalue ψ_0, the size of the rod is determined. Since the period is set to 1, the cross section of the rod in the box is symmetric about $x = 1/2$, both $Y_{\max}$ and $Y_{\min}$ are located at $x = 1/2$. Therefore, we have:

$$4\cos\left(2\pi \cdot \frac{1}{2}\right) + 4\cos(2\pi y) + 3 = \psi_0$$

That is:

$$\cos(2\pi y) = \frac{\psi_0 + 1}{4}$$

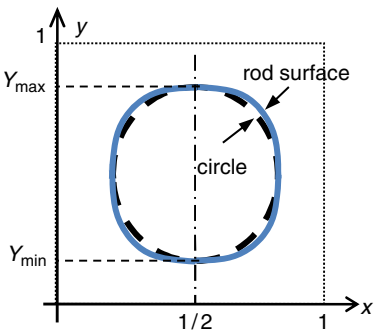

Figure 5.
Cylinder approximated by the rod surface

There are two solutions for $y \in [0, 1]$, which are Y_{max} and Y_{min}. Thus, the diameter is:

$$D = Y_{max} - Y_{min} = 1 - \arccos\left(\frac{\psi_0 + 1}{4}\right)/\pi \tag{5}$$

For example, when $\psi_0 = 0$, the diameter is approximately 0.58. Conversely, given a known diameter D, the isovalue is calculated as:

$$\psi_0 = 4\cos[\pi(1-D)] - 1 \tag{6}$$

With properly chosen parameters, the PS model is also able to construct rod surfaces with varied cross-sections in order to model compressed fibers. For example:

$$\psi(x,\ y,\ z) = 4\cos(2\pi x) + \cos(3\pi x) + 4\cos(2\pi y) + \cos\left(\frac{\pi y}{6}\right) + \frac{1}{4}\cos(3\pi(x+z)) + 2.5 = 0,$$

models the compressed rod surface shown in Figure 6(a), and:

$$\psi(x,\ y,\ z) = 7\cos(2\pi x) + 7\cos(2\pi y) + 2\cos(4\pi x) + 2\cos(4\pi y) + 8 = 0$$

models the one shown in Figure 6(b). It is seen that the deformation can be modeled by increasing the scales and degrees, i.e. introducing more terms in the PS model.

The fiber model in Equation (4) is located at the center of the RVE. Transformation operations are needed if we need to generate models at other locations or with different orientations. It has been demonstrated that the transformation of a PS model is equivalent to the transformation of its basis vectors (Wang, 2007a, b). Therefore, the position and orientation of a fiber can be adjusted through the translation and rotation of the basis vectors $\mathbf{p}_m$'s.

In the RVE, a certain number of fibers can be generated with random values of orientations and locations. n fibers can be combined using the union operation as:

$$\psi_{(\cup)}(x,y,z) = \min\begin{pmatrix} \psi_1(x,y,z), \ldots, \psi_i(x,y,z), \\ \ldots, \psi_n(x,y,z) \end{pmatrix} \tag{7}$$

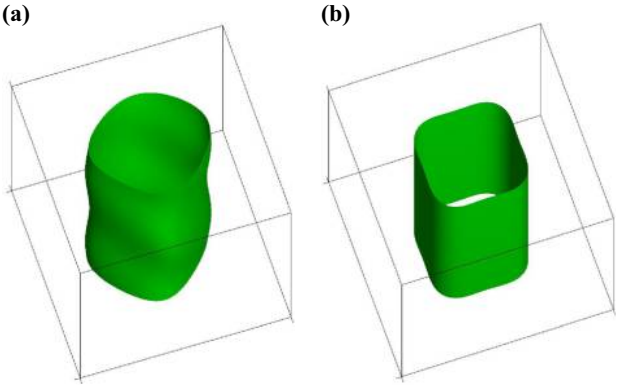

Figure 6.
Two compressed rod surfaces

where $\psi_i(x, y, z)$ is the PS model of the ith fiber. The randomly generated fibers in the PS model could intersect with each other. However, in reality, the fibers do not intersect. Instead, they bend when coming across with each other. Therefore, to better model the geometry, it is essential that the straight rod surface models are relocated and/or deformed, to avoid intersection. To quantify the intersection volume, we can use:

$$\psi_{(\cap)}(x,y,z) = \min_{1 \leqslant i < j \leqslant n} \left[\max\left(\psi_i(x,y,z), \psi_j(x,y,z)\right)\right] \tag{8}$$

The fiber positions and orientations should be adjusted to minimize the intersection portion. If $\mathbf{p}^{(i)} = \{\mathbf{p}_m^{(i)}\}$ denotes the collection of the basis vectors to model the ith fiber, this optimization problem can be described as:

$$\max_{\mathbf{p}^{(1)},\ldots,\mathbf{p}^{(n)}} \psi_{(\cap)}\left(x,y,z \middle| \mathbf{p}^{(1)}, \ldots, \mathbf{p}^{(n)}\right) \tag{9}$$

For fibers with deterministic patterns such as those in woven structures, the modeling and optimization procedures shown in Equations (7)-(9) still apply. After the optimization, the intersection portion among the fibers can be greatly reduced, which makes the model much closer to reality. It should be noted that the model we have now is based on the assumption that all fibers are straight. In order to build the bent rod model of fibers, the cross-section of the rod should shift by an amount varying along the rod axis. The shift amount here is directly related to the phase α_m in Equation (2). Therefore, we need to define α_m as a variable instead of a constant in the original PS model. To increase the flexibility, we generalize the PS model into a new form as described in the next section.

4. Generalized PS model

The generalized PS model is defined as:

$$\psi(\mathbf{r}) = \sum_{l=1}^{L}\sum_{m=1}^{M} \mu_{lm} \cos\left(\begin{array}{l} 2\pi\kappa_l\left(\mathbf{p}_m^T \cdot \mathbf{r}\right) + \\ \sum_{s=1}^{S}\sum_{t=1}^{T} u_{lmst} \cos\left(2\pi f_{lms}\left(\mathbf{q}_{lmt}^T \cdot \mathbf{r}\right)\right) \end{array}\right) = 0 \tag{10}$$

where $\mathbf{p}_m = [a_m,\ b_m,\ c_m,\ \alpha_m]^T = [\mathbf{H}_m,\ \alpha_m]^T$ remains the same as Equation (2), $\mathbf{q}_{lmt} = [e_{lmt}, f_{lmt}, g_{lmt}, \beta_{lmt}]^T = [\mathbf{G}_{lmt}, \beta_{lmt}]^T$, and $\mathbf{r} = [x, y, z, 1]^T$. Here $\mathbf{p}_m$'s are called major basis vectors and $\mathbf{q}_{lmt}$'s are minor basis vectors of the generalized PS model. μ_{lm}'s are now called major moments whereas u_{lmst}'s are minor moments. k_l's are major scales whereas f_{lms}'s are minor scales.

In the generalized PS model, the phase itself is a function with the similar form of the original PS model. That is, the phase is represented by cosine functions. As the phase now is not constant any more but a periodic function, the generalized PS model exhibits higher flexibility in modeling. In our fibrous porous media application, shown in Section 6, bent fibers can be efficiently represented. In a similar vein, we may even further parameterize the moments μ_{lm}'s in the PS model and make them as functions instead of constants as in Equations (1) and (10). The parameterization introduces more degrees of freedom to control the shapes of PS models.

In applications, rotational and translational operations on the generalized PS model are needed for interactive control. The two transformation operations are derived as in the following subsections.

4.1 Rotation of generalized PS model

After the rotation denoted by:

$$\mathbf{R}=\begin{bmatrix}\xi_{11} & \xi_{12} & \xi_{13} & \xi_{14}\\ \xi_{21} & \xi_{22} & \xi_{23} & \xi_{24}\\ \xi_{31} & \xi_{32} & \xi_{33} & \xi_{34}\\ \xi_{41} & \xi_{42} & \xi_{43} & \xi_{44}\end{bmatrix}$$

in which $\xi_{11}=\cos\theta\cos\omega$, $\xi_{12}=-\cos\theta\sin\omega$, $\xi_{13}=\sin\theta$, $\xi_{14}=0$, $\xi_{21}=\cos\varphi\sin\omega+\sin\varphi\sin\theta\cos\omega$, $\xi_{22}=\cos\varphi\cos\omega-\sin\varphi\sin\theta\sin\omega$, $\xi_{23}=-\sin\varphi\cos\theta$, $\xi_{24}=0$, $\xi_{31}=\sin\varphi\sin\omega-\cos\varphi\sin\theta\cos\omega$, $\xi_{32}=\sin\varphi\cos\omega+\cos\varphi\sin\theta\sin\omega$, $\xi_{33}=\cos\varphi\cos\theta$, $\xi_{34}=0$, $\xi_{41}=0$, $\xi_{42}=0$, $\xi_{43}=0$, $\xi_{44}=1$,where φ, θ and ω are the rotation angles about the x-, y- and z-axes respectively, the surface model $\psi(\mathbf{r})=0$ becomes $\psi(\mathbf{R}^{-1}\cdot\mathbf{r})=0$. That is:

$$\psi\left(\mathbf{R}^{-1}\cdot\mathbf{r}\right)=\sum_{l=1}^{L}\sum_{m=1}^{M}\mu_{lm}\cos\left(\begin{array}{l}2\pi\kappa_l\left(\mathbf{p}_m^T\cdot\mathbf{R}^{-1}\cdot\mathbf{r}\right)+\\ \sum_{s=1}^{S}\sum_{t=1}^{T}u_{lmst}\cos\left(2\pi f_{lms}\left(\mathbf{q}_{lmt}^T\cdot\mathbf{R}^{-1}\cdot\mathbf{r}\right)\right)\end{array}\right)=0$$

Since $\mathbf{R}^{-1}=\mathbf{R}^T$, we have:

$$\psi\left(\mathbf{R}^{-1}\cdot\mathbf{r}\right)=\sum_{l=1}^{L}\sum_{m=1}^{M}\mu_{lm}\cos\left(\begin{array}{l}2\pi\kappa_l\left((\mathbf{R}\cdot\mathbf{p}_m)^T\cdot\mathbf{r}\right)+\\ \sum_{s=1}^{S}\sum_{t=1}^{T}u_{lmst}\cos\left(2\pi f_{lms}(\mathbf{R}\cdot\mathbf{q}_{lmt})^T\cdot\mathbf{r}\right)\end{array}\right)=0 \quad (11)$$

It can be seen from Equation (11) that the rotation operation of the generalized PS model can be realized by the rotation of the major and minor basis vectors.

Furthermore, if we re-write each one of the basis vectors as the sum of two vectors with phase separated, i.e. $\mathbf{p}_m^T=[\mathbf{H}_m,a_m]=\mathbf{H}_m^*+\alpha_m^*$ where $\mathbf{H}_m^*=[\mathbf{H}_m,0]$ and $\boldsymbol{\alpha}_m^*=[\mathbf{0},a_m]$, and $\mathbf{q}_{lmt}^T=\left[\mathbf{G}_{lmt},\beta_{lmt}\right]=\mathbf{G}_{lmt}^*+\boldsymbol{\beta}_{lmt}^*$ where $\mathbf{G}_{lmt}^*=[\mathbf{G}_{lmt},0]$ and $\boldsymbol{\beta}_{lmt}^*=\left[\mathbf{0},\beta_{lmt}\right]$, then Equation (11) becomes:

$$\sum_{l=1}^{L}\sum_{m=1}^{M}\mu_{lm}\cos\left(\begin{array}{l}2\pi\kappa_l\left(\left(\mathbf{R}\cdot\mathbf{H}_m^{*T}\right)^T\cdot\mathbf{r}+\alpha_m\right)+\\ \sum_{s=1}^{S}\sum_{t=1}^{T}u_{lmst}\cos\left(2\pi f_{lms}\left(\mathbf{R}\cdot\mathbf{G}_{lmt}^{*T}\right)^T\cdot\mathbf{r}+\beta_{lmt}\right)\end{array}\right)=0$$

Because $\boldsymbol{\alpha}_m^*\cdot\mathbf{R}^T\cdot\mathbf{r}=\alpha_m$ and $\boldsymbol{\beta}_{lmt}^*\cdot\mathbf{R}^T\cdot\mathbf{r}=\beta_{lmt}$, a new form of the rotated generalized PS model is:

$$\sum_{l=1}^{L}\sum_{m=1}^{M}\mu_{lm}\cos\left(\begin{array}{l}2\pi\kappa_l\left(\left(\mathbf{R}\cdot\mathbf{H}_m^{*T}\right)^T\cdot\mathbf{r}+\alpha_m\right)+\\ \sum_{s=1}^{S}\sum_{t=1}^{T}u_{lmst}\cos\left(2\pi f_{lms}\left(\mathbf{R}\cdot\mathbf{G}_{lmt}^{*T}\right)^T\cdot\mathbf{r}+\beta_{lmt}\right)\end{array}\right)=0 \quad (12)$$

Equation (12) implies that the rotation operation does not change the phase of each cosine basis function.

4.2 Translation of generalized PS model

The translation operation can be derived similarly. When the translation matrix:

$$\mathbf{T} = \begin{bmatrix} \mathbf{I}_{3\times3} & \mathbf{t} \\ \mathbf{0} & 1 \end{bmatrix}$$

is applied, the new PS model is:

$$\psi\left(\mathbf{T}^{-1}\cdot\mathbf{r}\right) = \sum_{l=1}^{L}\sum_{m=1}^{M}\mu_{lm}\cos\left(\begin{array}{l} 2\pi\kappa_l\left(\mathbf{p}_m^T\cdot\mathbf{T}^{-1}\cdot\mathbf{r}\right)+ \\ \sum_{s=1}^{S}\sum_{t=1}^{T}u_{lmst}\cos\left(2\pi f_{lms}\left(\mathbf{q}_{lmt}^T\cdot\mathbf{T}^{-1}\cdot\mathbf{r}\right)\right) \end{array}\right) = 0$$

Let:

$$\mathbf{T}_t = \left(\mathbf{T}^{-1}\right)^T = \begin{bmatrix} \mathbf{I}_{3\times3} & \mathbf{0} \\ -\mathbf{t}^T & 1 \end{bmatrix}$$

the translated PS model is:

$$\psi\left(\mathbf{T}^{-1}\cdot\mathbf{r}\right) = \sum_{l=1}^{L}\sum_{m=1}^{M}\mu_{lm}\cos\left(\begin{array}{l} 2\pi\kappa_l\left(\left(\mathbf{T}_t\cdot\mathbf{p}_m\right)^T\cdot\mathbf{r}\right)+ \\ \sum_{s=1}^{S}\sum_{t=1}^{T}u_{lmst}\cos\left(2\pi f_{lms}\left(\left(\mathbf{T}_t\cdot\mathbf{q}_{lmt}\right)^T\cdot\mathbf{r}\right)\right) \end{array}\right) = 0$$

With basis vectors decomposed:

$$\sum_{l=1}^{L}\sum_{m=1}^{M}\mu_{lm}\cos\left(\begin{array}{l} 2\pi\kappa_l\left(\mathbf{H}_m^*\cdot\mathbf{T}^{-1}\cdot\mathbf{r}+\boldsymbol{\alpha}_m^*\cdot\mathbf{T}^{-1}\cdot\mathbf{r}\right)+ \\ \sum_{s=1}^{S}\sum_{t=1}^{T}u_{lmst}\cos\left(2\pi f_{lms}\left(\mathbf{G}_{lmt}^*\cdot\mathbf{T}^{-1}\cdot\mathbf{r}+\boldsymbol{\beta}_{lmt}^*\cdot\mathbf{T}^{-1}\cdot\mathbf{r}\right)\right) \end{array}\right) = 0$$

Similarly, because $\boldsymbol{\alpha}_m^*\cdot\mathbf{T}^{-1}\cdot\mathbf{r} = \alpha_m$ and $\boldsymbol{\beta}_{lmt}^*\cdot\mathbf{T}^{-1}\cdot\mathbf{r} = \beta_{lmt}$,

$$\sum_{l=1}^{L}\sum_{m=1}^{M}\mu_{lm}\cos\left(\begin{array}{l} 2\pi\kappa_l\left(\left(\mathbf{T}_t\cdot\mathbf{H}_m^*\right)^T\cdot\mathbf{r}+\alpha_m\right)+ \\ \sum_{s=1}^{S}\sum_{t=1}^{T}u_{lmst}\cos\left(2\pi f_{lms}\left(\left(\mathbf{T}_t\cdot\mathbf{G}_{lmt}^*\right)^T\cdot\mathbf{r}+\beta_{lmt}\right)\right) \end{array}\right) = 0$$

4.3 Calculation of the medial axis of generalized PS model

The medial axis is also known as topological skeleton and essential in model reconstruction, statistical distribution analysis, shape simplification, and other applications. In PS models, we may need to retrieve the medial axes of certain shapes for the purpose of

model reconstruction. For instance, when applying the generalized PS model in building fibrous porous media, we need to find the medial axes of fibers to reconstruct them in CFD analysis tools that do not support implicit modeling. For simple shapes such as sphere and rod, the medial axis is trivial. Here, we show the calculation of the medial axes of generalized PS models when there is only one term of basis function associated with μ_{lm} that contains variable phase. That is, there is only one combination of $l=l_0$ and $m=m_0$ such that not all $u_{lmst}=0$ among $s=1, \ldots, S$ and $t=1, \ldots, T$. For all other values $l\neq l_0$ or $m\neq m_0$, $u_{lmst}=0$. This is common when wavy shapes appear in generalized PS models along one direction without twists.

The medial axis of one directional wavy PS model can be computed by solving:

$$\begin{cases} \mathbf{p}_{m_0}^T \cdot \mathbf{r} - \sum_{s=1}^{S}\sum_{t=1}^{T} u_{l_0 m_0 st} \cos\left(2\pi f_{l_0 m_0 s}\left(\mathbf{q}_{l_0 m_0 t}^T \cdot \mathbf{r}\right)\right) = 0 \\ \hat{\mathbf{n}}^T \cdot \mathbf{r} = 0 \end{cases} \tag{13}$$

which correspond to a wavy surface and a plane with the normal vector of $\hat{\mathbf{n}}$ respectively, both passing through the medial axis.

The explicit rotation and translation of the medial axis can also be conveniently computed by solving:

$$\begin{cases} \mathbf{p}_{m_0}^T \cdot \mathbf{R}^{-1} \cdot \mathbf{r} - \sum_{s=1}^{S}\sum_{t=1}^{T} u_{l_0 m_0 st} \cos\left(2\pi f_{l_0 m_0 s}\left(\mathbf{q}_{l_0 m_0 t}^T \cdot \mathbf{R}^{-1} \cdot \mathbf{r}\right)\right) \\ = 0 \\ \hat{\mathbf{n}}^T \cdot \mathbf{R}^{-1} \cdot \mathbf{r} = 0 \end{cases} \tag{14}$$

and:

$$\begin{cases} \mathbf{p}_{m_0}^T \cdot \mathbf{T}^{-1} \cdot \mathbf{r} - \sum_{s=1}^{S}\sum_{t=1}^{T} u_{l_0 m_0 st} \cos\left(2\pi f_{l_0 m_0 s}\left(\mathbf{q}_{l_0 m_0 t}^T \cdot \mathbf{T}^{-1} \cdot \mathbf{r}\right)\right) \\ = 0 \\ \hat{\mathbf{n}}^T \cdot \mathbf{T}^{-1} \cdot \mathbf{r} = 0 \end{cases} \tag{15}$$

where $\mathbf{R}$ is the rotation matrix and $\mathbf{T}$ is the translation matrix.

5. Modeling bent fibers using generalized PS model

We use a generalized PS model to represent bent fibers. Here we call it bent rod surface. The shape of the cross section of the rod surface is largely determined by the parameters μ_{lm}, κ_l and $\mathbf{p}_m$, whereas the extension of bending is determined by the parameters u_{lmst}, f_{lms} and $\mathbf{q}_{lmt}$ in Equation (10). Since the cross section of the simple rod surface in Equation (4) is a good approximation of a circle, the parameters of μ_{lm}, κ_l and $\mathbf{p}_m$ can be remained the same for the bent ones. The relationship between the diameter of a bent rod and the isovalue can still be represented as in Equations (5) and (6).

For woven yarns in regular patterns, the bent shapes of the component fibers subject to external constraints can be approximated by the method of minimum energy (e.g. Hearle and Shanahan, 1978). Here we use a simple generalized PS model with $S=1$ and $T=1$ to model the bent fiber. The phase function is simply $u\cos(2\pi f(\mathbf{q}^T\ \mathbf{r})$. The bent rod surface:

$$\psi(x,y,z) = 4\cos(2\pi x + u\cos(2\pi f z)) + 4\cos(2\pi y) + 3 = \psi_0 \tag{16}$$

has the medial axis in the x-z plane with the specified parameters of u and f, and the resulted model has a sinusoidal shape as shown in Figure 7, where u determines the amplitude and f determines the frequency of vibration. Here the medial axis is actually the central curve passing through the centers of all the cross sections. For the central curves of bent rod surfaces oriented in the x-y and y-z planes, the respective major and minor basis vectors are $\mathbf{p}_1=[0\ 1\ 0\ 0]^T$, $\mathbf{p}_2=[0\ 0\ 1\ 0]^T$, $\mathbf{p}_3=[0\ 0\ 0\ 0]^T$, $\mathbf{q}_{111}=[1\ 0\ 0\ 0]^T$ and $\mathbf{p}_1=[1\ 0\ 0\ 0]^T$, $\mathbf{p}_2=[0\ 0\ 1\ 0]^T$, $\mathbf{p}_3=[0\ 0\ 0\ 0]^T$, $\mathbf{q}_{111}=[0\ 1\ 0\ 0]^T$. For the central curves of bent rod surfaces oriented in other planes, the basis vectors can be obtained through the rotation operation introduced in the previous section. It should be noticed that as more cosine basis functions are added for the phase, the shape of the fiber will be more flexible at the cost of computation. The carbon fibers in GDL we study in this paper are brittle and merely slightly bent when compressed. The wave length corresponding to the minor scale in the generalized PS model thus is large. In one RVE, there are usually only no more than two wave sections. Consequently, a single term of basis function is good enough for shape approximation of bent carbon fibers.

The generalized PS model of bent fibers presented here is an approximation based on geometry only. The more accurate models for shape changes as the result of external loads require mechanics analysis with the consideration of material properties. In Section 7, we will describe a new physics-based empirical force field method that models fiber bending and deformation based on the generalized PS model with implicit form.

When the cross-sections of the straight rod shift with an amount of $u\cos(2\pi f(\mathbf{q}^T\cdot\mathbf{r})$ to form a bent one, the actual cross-sections change slightly at the same time. As illustrated in Figure 8, when the cross section CS_2 shifts at a distance of v, the cross

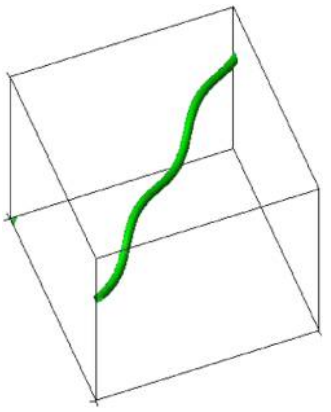

Figure 7.
A bent rod surface model with a sinusoidal shape

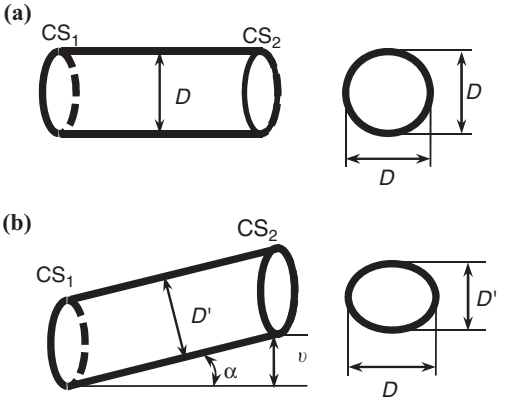

Figure 8.
Illustration of the cross-section change due to the shift

Notes: (a) Geometry and cross-section before shift; (b) geometry and cross-section after shift

section of the rod surface changes to a new shape, and the narrowest diameter changes from D to $D' = D\cos\alpha$. Then the difference between D and D' is $D_{diff} = D - D' = D(1-\cos\alpha)$. When the bent shape is $u\cos(2\pi f(\mathbf{q}^T \cdot \mathbf{r})$, the maximum value of α is $\alpha_{\max} = \arctan u$, and the maximum difference is:

$$D_{diff-\max} = D - D' = D \cdot (1 - \cos\alpha_{\max}) = D \cdot (1 - \cos(\arctan u))$$

In the case that the bending is slight, the amplitude a is small, therefore $D_{diff-\max}$ can be negligible. For instance, when a is 0.1, $D_{\text{diff}-\max} = 0.00496D$.

The generalized PS model can be used to model the compressed bent fibers. Figure 9 (a) shows a bent fiber with compressed cross-sections at certain contact positions with other fibers in the domain of $x \in [0, 1]$, $y \in [0, 1]$, and $z \in [0, 3]$. The construction process is as follows. From the straight fiber model in Equation (4), we would like to change the

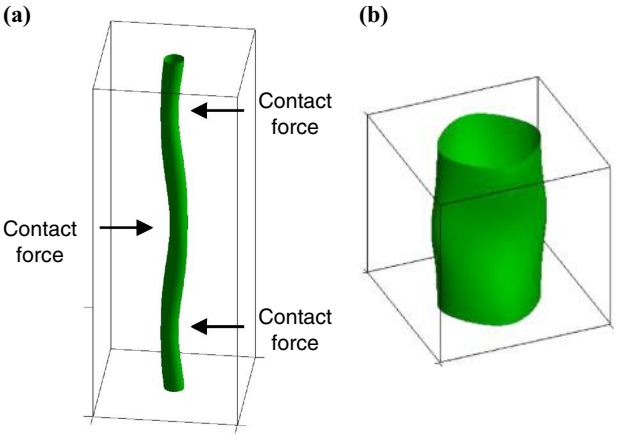

Figure 9.
Modeling a compressed bent fiber

Notes: (a) Geometric model; (b) enlarged compressed portion

cross-section periodically along the z direction. At the same time, the isovalue needs to be modified to a function of the z coordinate. Therefore, the model becomes:

$$\psi(x,y,z) = 4\cos(2\pi x) + \cos(2\pi y)(\cos(2\pi z)+3) + 0.95\cos(2\pi z) + 6.55 = 0$$

which is transformed into the generalized PS model of:

$$\psi(x,y,z) = 4\cos(2\pi x) + 3\cos(2\pi y) + 0.95\cos(2\pi z) + 0.5\cos(2\pi(y+z)) + 0.5\cos(2\pi(y-z)) + 6.55 = 0 \quad (17)$$

The bent rod surface model of Equation (17) is then incorporated into Equation (17), and the period and phase of the bent rod surface model are adjusted so that the contact and bending positions are overlapped. The resulted PS model is:

$$\psi(x,y,z) = 4\cos\left(2\pi x + 0.3\cos\left(\pi z - \frac{\pi}{2}\right)\right) + 3\cos(2\pi y) + 0.95\cos(2\pi z) + 0.5\cos(2\pi(y+z)) + 0.5\cos(2\pi(y-z)) + 6.55 = 0 \quad (18)$$

The detailed deformation at the contact positions is shown in Figure 9(b).

Based on the compressed bent fibers, woven fibers can be modeled. When the major scale parameters of the model in Equation (18) are modified, the model becomes:

$$\psi(x,y,z) = 4\cos\left(2\pi x + 0.41\cos\left(3\pi z - \frac{\pi}{2}\right)\right) + 3\cos(2\pi y) + 0.95\cos(6\pi z) + 0.5\cos(2\pi(y+3z)) + 0.5\cos(2\pi(y-3z)) + 6.55 = 0 \quad (19)$$

for one fiber. The example of woven fibers shown in Figure 10 has six fibers with translations and rotations applied to the fiber model in Equation (19) within the domain of $x \in [0,1]$, $y \in [0,1]$, and $z \in [0,1]$. It can be seen that at the contact locations, fibers are compressed and deformed accordingly. For each fiber, the locations where it is compressed are modeled by controlling the major scale parameters, whereas the bending is controlled separately by the minor scale parameters. The orientation and translation of fibers are calculated so that fibers are properly crossed or parallel. The rotations are 90 degree. The corresponding translation vectors of the six fibers are listed in Table I. Again, the deformed shape is an approximation of geometry rather than the result of physics-based modeling.

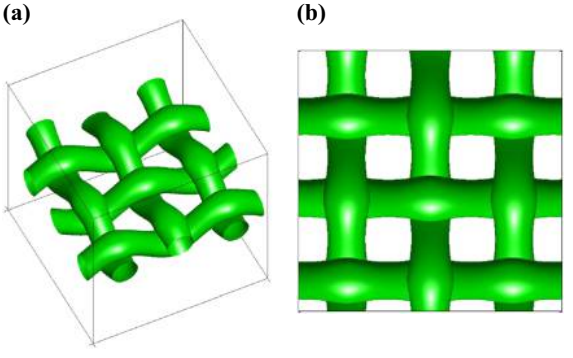

Notes: (a) Isometric view; (b) top view

Figure 10.
A PS model of woven fibers

6. Physics-based empirical force field to model fiber bending and deformation

In the physical world, systems tend to stabilize at the configurations with minimum potential energies. This general principle can be used to model the shape deformation of fibers with better approximations of the real shape. This requires a well-defined function of potential energy for fibers in terms of the shape parameters, i.e. the major and minor basis vectors, in the PS model. Then the shape parameters are optimized to obtain the minimum potential energy.

If external forces are removed during assembly, fibers, either woven or non-woven, tend to recover to a stable state with the minimum potential energy. The fibers are bent, and the cross-sections are compressed at the contact points. The fibers should also be contacting each other at the bent and compressed locations, and dangling is not acceptable. In addition, the fibers tend to have deformation that is as small as possible. Therefore, the surface area of the fibers should be minimized. Based on these principles, the total potential U of assembled fibers is defined as the sum of a pair-wise volume interaction potential, a surface interaction potential, and a surface potential. These potential energy functions are defined as follows.

The pair-wise volume interaction potential is defined as $I_{ij}^{(V)} = -\int_{\psi_{i\cap j}(\mathbf{r}) \leqslant 0} \psi_{i\cap j}(\mathbf{r}) d\mathbf{r}$. It is to measure the interaction between two fibers ψ_i and ψ_j in order to avoid intersection. The surface interaction potential is defined as $I_j^{(S)} = \oint_{\psi_j=0} \psi_{\cup j}(\mathbf{r}) d\mathbf{r}$, where $\psi_{\cup j}$ is the equivalent field of all fibers with the jth one excluded. It is to ensure physical contact of the jth fiber with others so that no fibers are dangling in the air. The surface potential is defined as $S_j = \oint_{\psi_j=0} K_j(\mathbf{r}) d\mathbf{r}$, where K_j is the Gaussian curvature on a point on the surface of the ith fiber. It is to ensure that the fibers have the minimum surface area so that they have the minimum amount of deformation.

Therefore, the total potential can be written as $U = w_1 \sum_{i<j} I_{ij}^{(V)} + w_2 \sum_j I_j^{(S)} + w_3 \sum_j S_j$, where w_1, w_2 and w_3 are the weights for pair-wise volume interaction potential, surface interaction potential and surface potential, respectively.

The general optimization problem to find the stable configuration can be formulated as:

$$\min_{\mu,\ \kappa,\ u,f,\ t_x,\ t_y,\ t_z} U(\mu, \kappa, u, f, t_x, t_y, t_z)$$

$$s.t. f > 0$$

where μ, κ, u, f, t_x, t_y and t_z are major moments, major scale parameters, minor moments, minor scale parameters, and translation vectors respectively for all fibers in the system.

Table I. Translation vectors of the six woven fibers

Fiber number	Translation vector coordinates X	Y	Z
1	0.41	−0.318	0
2	0.72	0	0
3	0.41	0.318	0
4	0.38	0.204	0
5	0.33	−0.433	0
6	0.28	0.204	0

The possible major and minor basis vectors are pre-determined before optimization. Initially all moments could be zeros. After optimization, if a moment is zero, the corresponding basis vector has no effect on the final shape of fibers.

Because the shape parameters of the fibers are optimized to simulate the local deformation at the contact points, local optimization methods are suitable similar to the traditional variational formulation. In the remainder of this section, we use two examples to illustrate the formulation.

6.1 Two-fiber assembly

The first example is given as a two-fiber assembly. The initial condition is that two fibers in the same plane are coming across each other. The two fibers have 90° difference of orientation around the out-of-plane direction, as shown in Figure 11(a). In reality, the two fibers will not intersect with each other. Instead, they will bend and deform to avoid each other. In our formulation, the locations and orientations of the two fibers are fixed. Therefore, when the shape of the fibers is approximated as a sinusoidal function, the optimization parameters are the scale parameters f_1 and f_2, and periodic moments u_1 and u_2. As stated in Section 6, f determines the frequency of vibration, and u determines the amplitude. As a constraint to ensure the geometric symmetry of the assembly because of the symmetric compression load, the scale parameters of the two fibers are set to be the same, and the minor moments of the two fibers are set to have the same absolute value. Therefore, the only optimization parameters are the minor scale parameter f, and minor moments u_1 and u_2. The optimization problem can be formulated as:

$$\min_{u_1,\, u_2,\, f} U(u_1, u_2, f)$$

$$s.t. |u_1| = |u_2|,\ f > 0$$

The isovalue of the model is set as −8.82 to decide the fiber diameter. The initial values for the moments are set as zeros, and the scale parameter is set as a random value between 1 and 2. The adjustment ranges for the scale parameter and moments are [−1, 1] and [−0.2, 0.2], respectively. When $w_1 = 10^{10}$, $w_2 = 1$, and $w_3 = 1$, the result of the optimization is $f = 2.6733$, $u_1 = 0.1896$ and $u_2 = -0.1896$. The optimized model is shown in Figure 11(b). The Pattern search method is used. The CPU time is about four minutes on a PC.

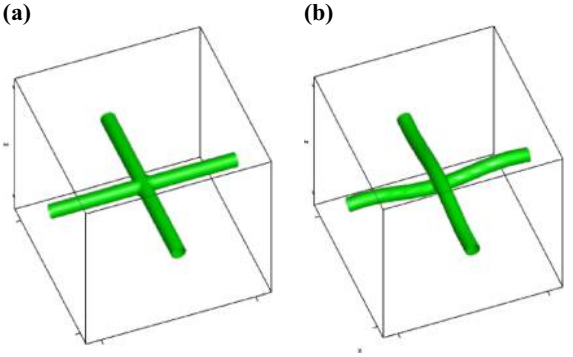

Notes: (a) Initial condition; (b) optimized deformation model with the empirical force field formulation

Figure 11. The deformation of two intersecting fibers in the same location but with 90° difference of orientation around the z-direction

6.2 Six-fiber woven assembly

The second example is given as a six-fiber woven assembly similar to Figure 10, where the fibers have compressed cross-sections. As stated in Section 4, the more terms are introduced into the PS model, the higher accuracy the shape has. However, for optimization purpose, the general PS model for a compressed bent fiber is formulated as:

$$\begin{aligned}\psi(x,y,z) = {} & \mu_1 \cos\left(2\pi\kappa_1\left(\mathbf{p}_1^T\cdot\mathbf{T}^{-1}\cdot\mathbf{r}\right)+u\cos\left(2\pi f\left(\mathbf{q}^T\cdot\mathbf{T}^{-1}\cdot\mathbf{r}\right)\right)\right)\\ & +\mu_2\cos\left(2\pi\kappa_2\left(\mathbf{p}_2^T\cdot\mathbf{T}^{-1}\cdot\mathbf{r}\right)\right)+\mu_3\cos\left(2\pi\kappa_3\left(\mathbf{p}_3^T\cdot\mathbf{T}\cdot\mathbf{r}\right)\right)\\ & +\mu_4\cos\left(2\pi\kappa_4\left(\mathbf{p}_4^T\cdot\mathbf{T}^{-1}\cdot\mathbf{r}\right)\right)+\mu_5\cos\left(2\pi\kappa_5\left(\mathbf{p}_5^T\cdot\mathbf{T}^{-1}\cdot\mathbf{r}\right)\right)=\text{isovalue}\end{aligned}$$

During optimization, the major basis vectors $\mathbf{p}$ and the minor basis vector $\mathbf{q}$ are fixed empirically as: $\mathbf{p}_1^T=[1,0,0,0]$, $\mathbf{p}_2^T=[0,1,0,0]$, $\mathbf{p}_3^T=[0,0,1,0]$, $\mathbf{p}_4^T=[0,1,1,0]$, $\mathbf{p}_5^T=[0,1,-1,0]$, and $\mathbf{q}_T=\left[0,0,1,-\frac{1}{6}\right]$, as in Equation (18). The isovalue is set for a desired diameter. All other variables are parameters to be optimized. As an example, when there is no translation, i.e. $\mathbf{t}=\mathbf{0}$ and $\mathbf{T}^{-1}=\mathbf{I}_{4\times4}$:

$$\begin{aligned}\psi(x,y,z) = {} & \mu_1\cos\left(2\pi\kappa_1 x+u\cos\left(2\pi f\left(z-\frac{1}{6}\right)\right)\right)+\mu_2\cos\left(2\pi\kappa_2 y\right)\\ & +\mu_3\cos\left(2\pi\kappa_3 z\right)+\mu_4\cos\left(2\pi\kappa_4(y+3z)\right)\\ & +\mu_5\cos\left(2\pi\kappa_5(y-3z)\right)=\text{isovalue}\end{aligned}$$

The parameters are not independent in this woven fiber example. Constraints need to be added. For instance, the fibers should have the largest deformation at those contact positions. The fibers should also be braided as a net with a symmetric pattern, and they have an identical shape. Therefore, when the central curves of the fibers are approximated as sinusoidal functions, the six fibers should have the same scale parameters μ_1, μ_2, μ_3, μ_4, μ_5, f, the same major moments κ_1, κ_2, κ_3, κ_4, κ_5, and the same absolute value of minor moment u. Furthermore, in order to guarantee that the six fibers are bent in a coordinated woven pattern, two adjacent fibers in the same direction should always have the opposite value of minor moment u. In addition, the orientations of the six fibers are fixed to form the woven pattern. The three fibers along the x-axis, i.e. fibers 1-3 in Table I, have a fixed location, whereas the other three fibers along the y-axis, i.e. fibers 4-6, have a variable translation of $\mathrm{t}=[t_x, t_y, 0]$ in the x-y plane. However, the distances between adjacent fibers in both directions are the same and fixed.

Therefore, the optimization problem can be formulated as:

$$\min_{\substack{\mu_1,\mu_2,\mu_3,\ \mu_4,\mu_5,\\ \kappa_1,\kappa_2,\kappa_3,\kappa_4,\kappa_5,\\ u_1,u_2,f,t_x,t_y}} U\left(\begin{matrix}\mu_1,\mu_2,\mu_3,\ \mu_4,\mu_5,\kappa_1,\kappa_2,\kappa_3,\kappa_4,\kappa_5,\\ u_1,u_2,f,t_x,t_y\end{matrix}\right)$$

$$s.t.\ \ \mu_1-\mu_2=1,\quad \mu_4=\mu_5,\quad \kappa_3=3\kappa_1=3\kappa_2=3\kappa_4=3\kappa_5,$$
$$f=1.5\kappa_1>0,\quad u_1=-u_2$$

where the constraints $\mu_1-\mu_2=1$, $\mu_4=\mu_5$, $\kappa_3=3\kappa_1=3\kappa_2=3\kappa_4=3\kappa_5$, and $f=1.5\kappa_1>0$ are set based on the above considerations.

The isovalue of the model is set as −6.65 to decide the fiber diameter. The initial values and the adjustment ranges for the parameters are listed in Table II. In addition, the initial translation vectors for fibers 4-6 are (0.45, −0.28, 0), (0.45, 0.038, 0) and (0.45, 0.356, 0) respectively. The model of the initial condition is shown in Figure 12(a) and (b). Pattern search method is used for local optimization. When $\omega_1=10^{10}$, $\omega_2=1$ and $\omega_3=1$, the result parameters are listed in Table II. In addition, the initial translation vectors for fibers 1-3 are (0.45, −0.28, 0), (0.45, 0.038, 0) and (0.45, 0.356, 0), respectively. The optimized model is shown in Figure 12(c) and (d). The CPU time is about eight minutes on a PC.

The major limitation of the proposed empirical force field method is that the initial parameter values are pre-determined by an empirical way. If the parameters are independent, the solution space has very high dimensions. The relationship between the parameters and the geometry are not completely understood. Therefore, the optimum solution may not be physical. Therefore empirical knowledge as the extra constraints is needed in the optimization formulation.

7. Implementation and demonstration

The generalized PS models of woven and non-woven fibers are implemented in our software package, PSLab, in the MATLAB environment. Here we use the GDL carbon fibers as an example to demonstrate how random fibers are modeled. The PS models of porous media can be integrated with CFD analysis. We also show the analysis results of woven and non-woven fibers.

7.1 Geometric modeling of random non-woven fibers

The construction process for random non-woven fibers is as follows. The fibers are all initially oriented along the x-axis and located in the center of the RVE, then translated to the origin of the RVE and rotated about the y-axis by the angle of θ and z-axis by the angle of ω, followed by a translation by the vector (t_x, t_y, t_z). For the carbon fibers in Figure 2, the values of θ, ω and t_x, t_y, t_z are random and the ranges are $\theta\in[-5\pi/180, 5\pi/180]$, $\omega\in[0, \pi]$ and $t_x, t_y, t_z\in[0, 1]$, respectively. During the optimization in Equation (9), the objective function is the volume of intersection portion Ω, and the optimization

		Initial condition	Adjustment range	Optimization result
μ	μ_1	3.9	[−0.2, 0.2]	4.08
	μ_2	2.9		3.08
	μ_3	1.1		0.9750
	μ_4	0.55		0.4549
	μ_5	0.55		0.4549
κ	κ_1	0.9	[−0.3, 0.3]	0.96
	κ_2	0.9		0.96
	κ_3	2.9		2.88
	κ_4	0.9		0.96
	κ_5	0.9		0.96
u		0.29	[−0.2, 0.2]	0.415
f		1.3	[−0.3, 0.3]	1.44

Table II. The comparison of the initial condition and optimization result and the parameter adjustment ranges

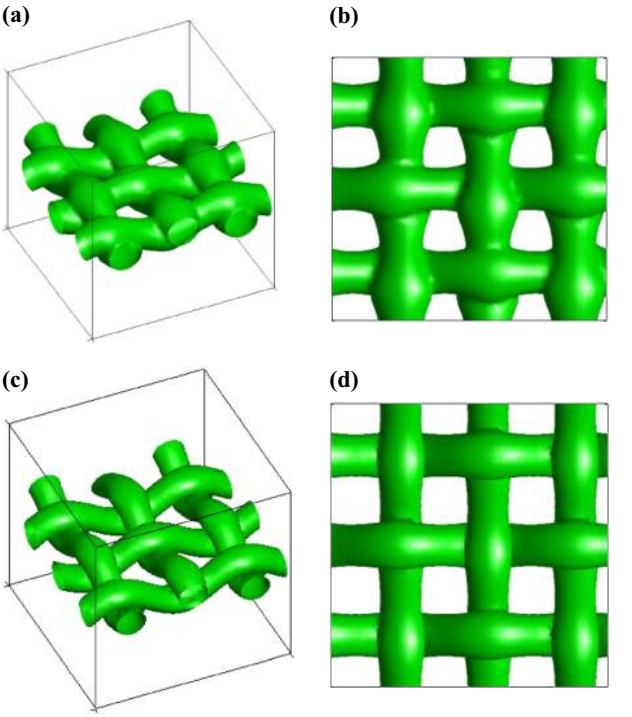

Notes: (a) The isometric view of the initial condition; (b) the top view of the initial condition; (c) the isometric view of the optimized deformation model using empirical force field method; (d) the top view of the optimized deformation model using empirical force field method

Figure 12.
The deformation of six woven fibers

parameters are θ, ω, t_x, t_y, and t_z. The volume Ω can be estimated by the number of voxels inside the isosurface of Ω. For the model of straight fibers, the optimization problem is formulated as:

$$\min_{\theta,\,\omega,\,t_x,\,t_y,\,t_z} \Omega(\theta, \omega, t_x, t_y, t_z)$$

For the model of bent fibers, there are two more parameters to be optimized, which are u and f. The optimization problem becomes:

$$\min_{u,\,f,\,\alpha,\,\beta,\,t_x,\,t_y,\,t_z} \Omega(u, f, \alpha, \beta, t_x, t_y, t_z)$$

Genetic algorithms are used to solve the optimization problem in implementation. Our preliminary study compared genetic algorithms with other methods such as particle swarm optimization and gradient-based local search, which showed that genetic algorithms have better results and higher time efficiency. The outputs of the function are the adjustment values of the initial random values. The adjustment ranges

of θ, ω, t_x, t_y, and t_z are set to be $[-\pi/180, \pi/180]$, $[-\pi/180, \pi/180]$, $[-0.1, 0.1]$, $[-0.1, 0.1]$ and $[-0.1, 0.1]$, respectively.

For the model of bent fibers, the adjustment range of additional parameters u and f are $u \in [0.1, 0.3]$, $f \in [1, 10]$, respectively . When $u = f = 0$, the model of the fiber is straight.

An example of PS models to represent straight fibers is illustrated in Figure 13. The medial axis of a straight fiber, which is required to reconstruct geometries in CFD analysis tools, is a straight line and thus can be represented by the position of any point on the axis of the fiber, such as the central point, and the axial orientation. Therefore, after optimization, the center positions and axial orientation vectors of the fibers are calculated for the subsequently reconstructed model in ANSYS/Fluent, the CFD tool used in this work. The center position of a fiber is calculated through the translation of the initial center position (1/2, 1/2, 1/2) in the RVE domain of the unit lengths; the axial orientation vector is calculated through the rotation of the initial axis vector of (1, 0, 0). This geometric information is then exported and imported to ANSYS/Fluent to reconstruct the geometry for CFD analysis. Volumetric mesh of the pore space is generated by GAMBIT software, as shown in Figure 14.

For bent fibers, Equation (16) is used. The medial axes of bent rod surfaces are also needed to export the model to ANSYS/Fluent. An example of geometric model is shown

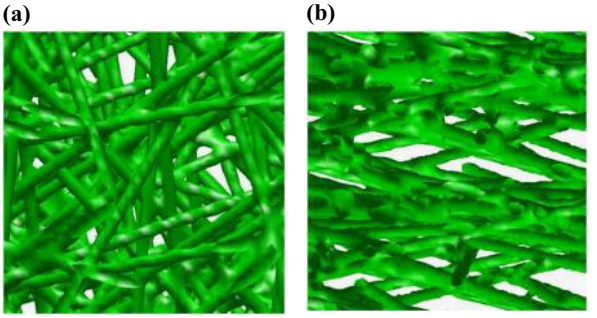

Notes: (a) Top view of fibers; (b) top view of rod surface model; (c) side view of fibers; (d) side view of rod surface model

Figure 13.
An example of straight rod PS surface models

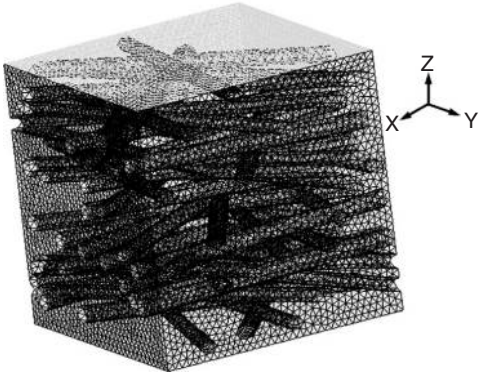

Figure 14.
Unstructured volumetric mesh of the porous media with the straight fibers for CFD analysis

in Figure 15(a). Following the procedure in Section 5.3, we first calculate the medial axes in their initial position located at the center of the RVE as in Equation (13), then find the new equations corresponding to the translated and rotated ones as in Equations (14) and (15). The initial medial axis used in this example is:

$$\begin{cases} z - \sin x = 0 \\ y = 0 \end{cases}$$

Once we have the closed-form mathematical expression of the medial axes, the curves are discretized and the locations of the sampled points are the inputs for CFD tools. Spline curves as the interpolated extrusion paths are then used to reconstruct fibers in ANSYS/Fluent. The unstructured volumetric mesh for the bent fibers model is shown in Figure 15(b). Similarly, the mesh model for woven fibers can be constructed. Figure 16 shows such an example.

For layered or strongly anisotropic fibrous structures, the distribution of fibers such as the ones in Figure 13 is not uniform any more. We can choose any appropriate distributions to generate fibers in the model. Figure 17 gives an example of 20 bent fibers with translations in the z direction with a beta distribution (parameters $a = 4$ and $b = 4$) instead of the uniform one. In such non-uniform fiber distributions, fibers are more dense at the center location of the RVE. In order to conform certain distributions even after the optimization procedure to reduce intersection, some lower and upper bounds of translations for fibers can be set up. Figure 18 gives another example of 20 bent fibers with the rotation angles following an exponential distribution with

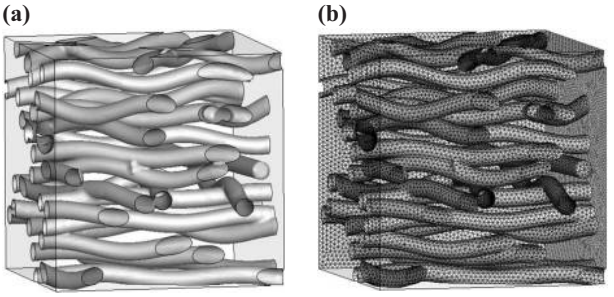

Notes: (a) Geometric model; (b) unstructured volumetric mesh

Figure 15.
Modeling bent fibers for CFD analysis

Figure 16.
An example of volumetric meshes for woven fibers

parameter $\mu = 0.4$. Therefore, different probability density functions can be applied to represent distributions of fibers in different scenarios.

7.2 CFD analysis

To check the accuracy of the proposed modeling technique, the flow field inside the pore space of the three types of fibrous media (straight, bent, and woven) was modeled. The through-plane and in-plane permeability values were calculated.

To find the proper size of the RVE for accurate CFD analysis, the Brinkman screening length criterion (Clague *et al.*, 2000) is used. Based on the reported values (Caston *et al.*, 2011; Gostick *et al.*, 2006) for the GDL's permeability, a cube with the length of 100 μm is large enough to smooth out the local non-homogeneities in the porous media.

After generating the fibrous micro-structures and the volumetric tetrahedral meshes for the pore space as shown in Figures 14 and 15. The mass and momentum equations are solved by the finite volume method in the ANSYS/Fluent software. The momentum equation is discretized by the second order upwind scheme with the SIMPLE algorithm for the pressure-velocity coupling. The under relaxation factors of 0.25 and 0.55 for pressure and momentum are used, respectively. The convergence criteria of 10^{-6} for

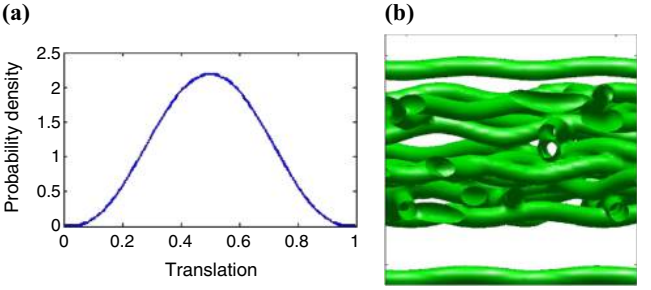

Notes: (a) The probability density function of the β distribution with a = 4 and b = 4; (b) the resulted model of bent fibers

Figure 17. Modeling bent fibers with a beta distribution of translations in the z direction

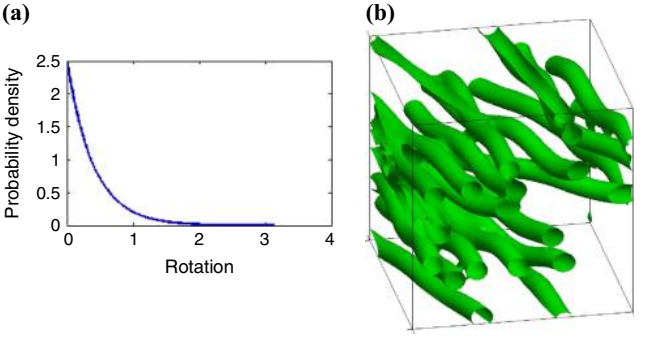

Notes: (a) The probability density function of the exponential distribution with $\mu = 0.4$; (b) the resulted model of bent fibers

Figure18. Modeling bent fibers with an exponential distribution of rotations

the momentum and mass conservation equations are used. The permeability (K) of the porous media is found from Darcy's law:

$$V = \frac{K}{\eta} \nabla P$$

where V is the superficial velocity (i.e. volumetric flow rate per unit cross sectional area), η is the fluid viscosity, and ∇P is the pressure drop per unit length through the porous material. An isometric view of the $100 \times 100 \times 100$ μm computational domain is shown in Figure 19. To determine the permeability in a desired direction, the inlet and outlet boundary conditions are set to the respective flow direction. At the inlet, a constant velocity perpendicular to the boundary is defined, whereas at the outlet, an outflow condition is imposed. No slip boundary condition is applied to the internal solid-fluid interface, which are the outer surfaces of the fibers. To minimize the end effects on the flow field, identical auxiliary zones at the inlet and outlet of the two opposite faces in the direction of interest are added to the main porous domain.

Toray 90 GDL was selected as the test sample for the non-woven structure. It has the porosity of 0.8 with the fiber diameter of 7 μm and the through-plane permeability of 8.3×10^{-12} m^2 as measured by Gostick *et al.* (2006). According to the experimental study conducted by Caston *et al.* (2011), the through-plane permeability of woven structure depends on the its woven patterns of the fabric. The range of the permeability is between 2×10^{-12} and 1×10^{-11} m^2. In our previous study (Didari *et al.*, 2012), it was shown that the higher the porosity is, the larger permeability value the fibrous porous media would have. As seen in Table III, the numerically estimated permeability values through the CFD analysis in our study are in a good agreement with the experimentally measured ones.

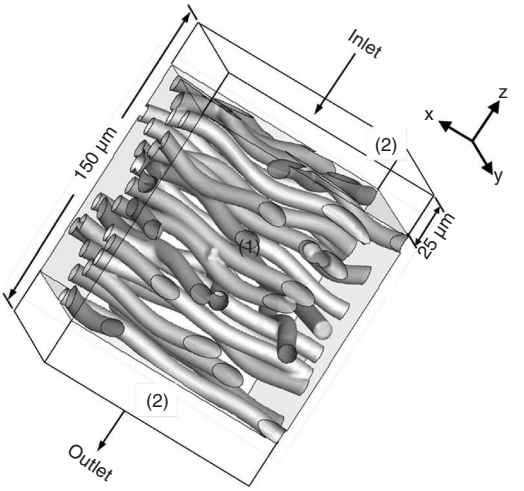

Figure 19.
The computational domain and boundary conditions for CFD analysis

Notes: Inlet: pressure boundary; outlet: overflow.
(1): porous domain; (2): auxiliary domain

8. Concluding remarks

In this paper, we proposed a generalized PS model and presented a new method to represent the geometry of microscopic fibrous porous media. The fibers in the models, either straight or bent, are efficiently constructed. The shape, position, and orientation of fibers are controllable to serve the purpose of design. Existing geometric modeling approaches are not suitable for modeling fibrous porous media for the purpose of design. In addition to the pure geometric modeling method, a physics-based empirical force field approach based on the principle of minimum potential energy is proposed to model the deformation of both woven and non-woven fiber assemblies. The uniqueness of this formulation is that it is based on implicit surface modeling. The proposed geometric modeling method effectively integrates with CFD analysis for design optimization. The modeling and simulation results match the physical experimental measurement well. Compared to existing modeling methods for fibrous porous media, the generalized PS model has several advantages. The implicit nature of the model enables it to build 3D porous and complex structures more efficiently than explicit modeling approaches. With global control of the shape, the macroscopic properties of porous media such as porosity and permeability can be linked to geometric parameters for ease of design. Furthermore, the model's inherent periodicity allows for creation of self-repeating geometry. Thus the size of the RVE is easily modifiable while its porosity is kept the same.

However, there are some limitations in our approach. In modeling the deformation of compressed fibers, the relationship between the parameters in the configuration space and the geometry in the Euclidean space is not completely understood. Therefore, the intuitive connection between the parameters and the shape is not available. In the future work, we want to establish the relationship between the parameters and the fiber shape. The computational load for the parameter optimization procedure is the major portion of computational cost in our method. The current implementation in Matlab is not necessarily optimized. Future study of computational efficiency is required if problems that are much larger than the ones in this paper need to be solved. Application specific optimization algorithms may be needed. In current empirical force field formulation, the weights associated with the three potential terms are determined empirically case-by-case. We would like to investigate a more systematic approach to determine them in the future. Furthermore, in this paper we construct the computational domain by retrieving the coordinates of medial axes from the surface models. In the future, we will also investigate the effective approach to export surface meshes directly to CFD tools so that geometries which are more complex than fibers can be modeled and simulated. The main challenge of this approach is to ensure the high quality of meshes that are directly generated from PS models such that the CFD analysis results are accurate.

Fiber type	Through-plane (m^2)	In-plane (m^2)
Straight	8.07×10^{-12}	1.21×10^{-11}
Bent	7.8×10^{-12}	1.11×10^{-11}
Woven	2.55×10^{-12}	n/a

Table III. Through-plane and in-plane permeability

References

Bentz, D.P., Quénard, D.A., Kunzel, H.M., Baruchel, J., Peyrin, F., Martys, N.S. and Garboczi, E.J. (2000), "Micro-structure and transport properties of porous building materials. II: three-dimensional X-ray tomographic studies", *Materials and Structures*, Vol. 33 No. 3, pp. 147-153.

Brown, R.C. (1984), "A many-fibre model of airflow through a fibrous filter", *Journal of Aerosol Science*, Vol. 15 No. 5, pp. 583-593.

Brown, R.C. (1993), "Theory of airflow through filters modelled as arrays of parallel fibres", *Chemical Engineering Science*, Vol. 48 No. 20, pp. 3535-3543.

Caston, T.B., Murphy, A.R. and Harris, T.A.L. (2011), "Effect of weave tightness and structure on the in-plane and through-plane air permeability of woven carbon fibers for gas diffusion layers", *Journal of Power Sources*, Vol. 196 No. 2, pp. 709-716.

Cheah, C.M., Chua, C.K., Leong, K.F. and Chua, S.W. (2003a), "Development of a tissue engineering scaffold structure library for rapid prototyping. Part 1: investigation and classification", *International Journal of Advanced Manufacturing Technology*, Vol. 21 No. 4, pp. 291-301.

Cheah, C.M., Chua, C.K., Leong, K.F. and Chua, S.W. (2003b), "Development of a tissue engineering scaffold structure library for rapid prototyping. Part 2: parametric library and assembly program", *International Journal of Advanced Manufacturing Technology*, Vol. 21 No. 4, pp. 302-312.

Chen, X. and Papathanasiou, T.D. (2005), "On the variability of the Kozeny constant for saturated flow across unidirectional disordered fiber arrays", *Composite Part A: Applied Science and Manufacturing*, Vol. 37 No. 6, pp. 836-846.

Chow, H.N., Tan, S.T. and Sze, W.S. (2007), "Layered modeling of porous structures with voronoi diagrams", *Computer-Aided Design & Applications*, Vol. 4 Nos 1/4, pp. 321-330.

Clague, D.S., Kandhai, B.D., Zhang, R. and Sloot, P.M.A. (2000), "Hydraulic permeability of (un) bounded fibrous media using the lattice Boltzmann method", *Physical Review E*, Vol. 61 No. 1, pp. 616-625.

Dabbs, D.M. and Aksay, I.A. (1996), "Structure and transport properties of porous. magnetic gel via x-ray microtomography", *Physical Review E*, Vol. 54 No. 3, pp. 2663-2669.

Desplentere, F., Lomov, S.V., Woerdeman, D.L., Verpoest, I., Wevers, M. and Bogdanovich, A. (2005), "Micro-CT characterization of variability in 3D textile architecture", *Composites Science and Technology*, Vol. 65 No. 13, pp. 1920-1930.

Didari, S., Harris, T.A.L., Huang, W., Tessier, S.M. and Wang, Y. (2012), "Feasibility of periodic surface models to develop gas diffusion layers: a gas permeability study", *International Journal of Hydrogen Energy*, Vol. 37 No. 19, pp. 14427-14438.

Flegler, S.L. (1993), *Scanning and Transmission Electron Microscopy: An Introduction*, Freeman, New York, NY.

Fredrich, T., Menendez, B. and Wong, T.F. (1995), "Imaging pore structure of geomaterials", *Science*, Vol. 268 No. 5208, pp. 276-278.

Gostick, J.T., Fowler, M.W., Pritzker, M.D., Ioannidis, M.A. and Behra, L.M. (2006), "In-plane and through-plane gas permeability of carbon fiber electrode backing layers", *Journal of Power Sources*, Vol. 162 No. 1, pp. 228-238.

Hamilton, D.J. (2005), "A numerical method to determine effective transport coeffcients in porous media with application to pem fuel cells", MSc thesis, Queen's University, Kingston.

Hearle, J.W.S. and Shanahan, W.J. (1978), "An energy method for calculations in fabric mechanics-Part I: principles and methods", *Journal of the Textile Institute*, Vol. 69 No. 4, pp. 81-91.

Herman, P.K., Lehmann, M.J. and Velu, Y.K. (2006), "Predicting initial pressure drop of fibrous media typical models and recent improvements", *Journal of Textile and Apparel, Technology and Management*, Vol. 5 No. 2, pp. 1-15.

Hewitt, J.A., Brown, D. and Clarke, R.B. (1995), "Computer modeling of woven composite materials", *Composites*, Vol. 26 No. 2, pp. 134-140.

Jaganathan, S., Tafreshi, H.V. and Pourdeyhimi, B. (2008), "A realistic approach for modeling permeability of fibrous media: 3-D imaging coupled with CFD simulation", *Chemical Engineering Science*, Vol. 63 No. 1, pp. 244-252.

Kinney, J.H. and Nichols, M.C. (1992), "X-ray tomographic microscopy (XTM) using synchrotron radiation", *Annual Reviews of Materials Science*, Vol. 22 No. 1, p. 121.

Kou, X.Y. and Tan, S.T. (2010a), "A simple and effective geometric representation for irregular porous structure modeling", *Computer-Aided Design*, Vol. 42 No. 10, pp. 930-941.

Kou, X.Y. and Tan, S.T. (2010b), "Modeling functionally graded porous structures with stochastic voronoi diagram and B-spline representations", *International Conference on Manufacturing Automation*, *Hong Kong*, pp. 99-106.

Lin, H.Y. and Newton, A. (1999), "Computer representation of woven fabric by using B-splines", *Journal of the Textile Institute*, Vol. 90 No. 1, pp. 59-72.

Peirce, F.T. (1937), "The geometry of cloth structure", *Journal of the Textile Institute*, Vol. 28 No. 3, pp. 45-96.

Qi, C. and Wang, Y. (2009), "Feature-based crystal construction with periodic surfaces", *Computer-Aided Design*, Vol. 41 No. 11, pp. 792-800.

Schroeder, C., Regli, W.C., Shokoufandeh, A., Sun, W. and Sun, E.W. (2003), "Representation of porous artifacts for biomedical applications", 8th ACM Symposium on Solid Modeling and Applications, Seattle, DC, pp. 254-257, available at: http://scholar.google.com/citations?view_op=view_citation&hl=en&user=CAWhuTkAAAAJ&citation_for_view=CAWhuTkAAAAJ:qjMakFHDy7sC

Schulz, V.P., Becker, J., Wiegmann, A., Mukherjee, P.P. and Wang, C.Y. (2007), "Modeling of two-phase behavior in the gas diffusion medium of PEFCs via full morphology approach", *Journal of the Electrochemical Society*, Vol. 154 No. 4, pp. 419-426.

Smith, M.A. and Chen, X. (2008), "CAD and constraint-based geometric modelling algorithms for 2D and 3D woven textile structures", *Journal of Information and Computing Science*, Vol. 3 No. 3, pp. 199-214.

Sreprateep, K. and Bohez, E.L.J. (2006), "Computer aided modeling of fiber assemblies", *Computer-Aided Design & Applications*, Vol. 3 Nos 1-4, pp. 367-376.

Stroscio, J.A. and Kaiser, W.J. (1992), *Scanning Tunneling Microscopy*, Academic, Boston, MA.

Strozzi, G., Marquez, J., Trujillo, F., Duwig, C., Prado, B., Gamage, P. and Delmas, P. (2009), "3D porous media liquid-solid interaction simulation using SPH modeling and tomographic images", *IAPR Conference on Machine Vision Applications*, *Yokohama*, Vol. 8 No. 30, pp. 328-331.

Sun, W., Lina, F. and Hu, X. (2001), "Computer-aided design and modeling of composite unit cells", *Composites Science and Technology*, Vol. 61 No. 2, pp. 289-299.

Sun, W., Starly, B., Nam, J. and Darling, A. (2005), "Bio-CAD modeling and its applications in computer-aided tissue engineering", *Computer-Aided Design*, Vol. 37 No. 11, pp. 1097-1114.

Turana, R.B. and Baser, G. (2010), "Three-dimensional computer simulation of 2/2 twill woven fabric by using B-splines", *Journal of the Textile Institute*, Vol. 101 No. 10, pp. 870-881.

Van Doormaal, M.A. and Pharoah, J.G. (2009), "Determination of permeability in fibrous porous media using the lattice boltzmann method with application to PEM fuel cells", *International Journal for Numerical Methods in Fluids*, Vol. 59 No. 1, pp. 75-89.

Vaughan, N.P. and Brown, R.C. (1996), "Observations of the microscopic structure of fibrous filters", *Filtration & Separation*, Vol. 33 No. 8, pp. 741-748.

Wang, Q., Vahedi Tafreshi, B.M.H. and Pourdeyhimi, B. (2006), "A case study of simulating submicron aerosol filtration via lightweight spun-bonded filter media", *Chemical Engineering Science*, Vol. 61 No. 15, pp. 4871-4883.

Wang, Y. (2007a), "Loci periodic surface reconstruction from crystals", *Computer-Aided Design & Applications*, Vol. 4 Nos 1/4, pp. 437-447.

Wang, Y. (2007b), "Periodic surface modeling for computer aided nano design", *Computer-Aided Design*, Vol. 39 No. 3, pp. 179-189.

Wang, Y. (2009), "Computing minkowski sums of periodic surface models", *Computer-Aided Design & Applications*, Vol. 6 No. 6, pp. 825-837.

Zeng, X., Vasseurb, C. and Fayalac, F. (2000), "Modeling microgeometric structures of porous media with a predominant axis for predicting diffusive flow in capillaries", *Applied Mathematical Modelling*, Vol. 24 No. 12, pp. 969-986.

Corresponding author
Dr Yan Wang can be contacted at: yan.wang@me.gatech.edu